ICHEP'96 Ref. pa01-061
Submitted to Pa 1, Pa 5, Pa 7
Pl 7, Pl 9

DELPHI 96-115 CONF 41
25 June, 1996

Measurement of the Partial Decay Width $R_b^0 = \frac{\Gamma_{b\bar{b}}}{\Gamma_{had}}$ with the DELPHI detector at LEP

Preliminary

DELPHI Collaboration

G.J.Barker, G.Borisov, C.De La Vaissiere, L.Lyons, M.Margoni, C.Mariotti, F.Martinez-Vidal, K.Moenig, A.M.Normand, P.Ronchese, F.Simonetto

Abstract

The DELPHI detector at LEP has recorded about 3 million hadronic Z decays during 1991–1994. From these data the branching ratio $Z \rightarrow b\overline{b}$ was measured by several methods. All methods heavily rely on the three layer silicon microvertex detector, sometimes complemented by event shapes or a high transverse momentum lepton tag. All methods measure R_b^0 together with the b-tagging efficiency by comparing single and double tag rates to reduce the systematic uncertainty.

This paper presents a new DELPHI analysis that measures R_b^0 from the 1994 data set using a decay length variable. The result is then combined with previous DELPHI results from the 1991–1993 data set to give the value:

$$R_b^0 = 0.2205 \pm 0.0014(\text{stat}) \pm 0.0018(\text{syst}) - 0.010\frac{R_c - 0.172}{0.172}.$$

1 Introduction

The partial decay width for $Z \rightarrow b\overline{b}$ in hadronic Z decays, $R_b^0 = \frac{\Gamma_{b\overline{b}}}{\Gamma_{had}}$, has been measured by LEP and SLD experiments with very good precision [1, 2, 3, 4, 5, 6]. The average value of R_b^0 [7] disagrees by about three standard deviations with the prediction of the Standard Model. A new analysis has been performed using data from the DELPHI experiment at LEP in order to study the observed deviation with a different systematic sensitivity. This paper presents this new measurement of the ratio of the cross-sections, $R_b = \frac{\sigma(Z \rightarrow b\overline{b})}{\sigma(Z \rightarrow hadrons)}$, using data taken during the 1994 run.

This analysis exploits the long lifetime of B-hadrons by reconstructing secondary vertices which are displaced from the primary vertex and tagging on the distance between the beamspot and the secondary vertex. A folded hemisphere double tagging technique is used to measure R_b and the b-tagging efficiency simultaneously from the data.

The result is then combined with the previous DELPHI number.

2 Event Selection

The DELPHI detector and its performance have been described in detail in ref. [8, 9].

The criteria to select charged tracks and to identify hadronic Z decays were identical to those described in [3]. Charged particles were accepted if:

- their polar angle was between 20° and 160°,
- their track length was larger than 30 cm,
- their impact parameter relative to the interaction point was less than 2.5 cm in the plane perpendicular to the beam direction (the $R\Phi$ plane) and less than 10 cm along the beam direction,
- their momentum was larger than 200 MeV/c with relative error less than 100%.

Neutral particles detected in the HPC were required to have measured energy larger than 700 MeV, and those detected in the EMF greater than 400 MeV.

Events were selected by requiring:

- at least 7 reconstructed charged particles,
- the summed energy of the charged particles had to be larger than 15% of the centre of mass energy, with at least 3% of it in each of the forward and backward hemispheres with respect to the beam axis.

The efficiency to find hadronic Z decays with these cuts was about 94% and all backgrounds were below 0.1%. After application of an event containment cut on the polar angle of the thrust axis, $|\cos\theta| < 0.65$, a selection bias towards $Z \rightarrow b\overline{b}$ events of (0.0012 ± 0.0002) was found. This was taken into account in the final result.

A sample of about twice the data statistics of $Z \rightarrow q\overline{q}$ events has been simulated using the Lund parton shower Monte Carlo JETSET 7.3 [10] (with parameters optimized by DELPHI) and the DELPHI detector simulation [11]. In addition, dedicated samples of $Z \rightarrow b\overline{b}$ events have been generated and used in order to reduce the error on the

correlation extracted from the simulation, which is dominated by the Monte Carlo statistical error. The simulated events have been passed through the same event reconstruction chain as the data.

3 The secondary vertex method

3.1 Vertex and Decay Length Fits

Before any attempt was made to find secondary vertices, jets were reconstructed within each event using a simple cone algorithm. Tracks were required to be within a cone of half-angle 0.5 rad around the reconstructed jet axis, and each jet had to have a minimum total energy, the sum of the energies of every charged and neutral particle associated with the jet, of 5 GeV. In about 1.1% of events only one jet was found. The average number of jets per event was 2.3. Different jet clustering algorithms were investigated but did not significantly influence the final result.

A secondary vertex fit was performed within each reconstructed jet from *physics* tracks which had passed the following tighter set of quality cuts:

- hits in at least 2 layers of the vertex detector (VD),
- an internal VD χ^2 [1] of less than 4,
- an impact parameter in the $R\Phi$ plane with respect to the beamspot of less than 0.15 cm,
- a momentum greater than 750 MeV/c.

In addition, an attempt was made to reconstruct tracks coming from decays of K^0_S and Λ particles and from photon conversions [9]. Such tracks were then rejected from the vertex fit.

The vertex fit was performed in the $R\Phi$ plane only using the following iterative procedure:

- all physics tracks in one jet were fitted to a common vertex, minimising

$$\chi^2 = \sum_{i=1}^{N} \frac{D_i^2}{\sigma_{D_i}^2}, \tag{1}$$

  where D_i is the distance of closest approach of the projection of track i in the $R\Phi$ plane to the candidate vertex and σ_{D_i} is the error on this distance;
- the track with the largest χ^2 was rejected if its contribution to the total was greater than 4;
- the vertex was refitted using the reduced track list and a new χ^2 was computed;
- the procedure continued until either all remaining tracks contributed less than 4 to the χ^2 or there were fewer than four tracks remaining.

[1] The VD χ^2 is defined as $\chi^2 = \Sigma_{tr}/N_{VD}$, where $\Sigma_{tr} = \sum d_i^2/\sigma_{VD}^2$. The sum is over all N_{VD} hits associated with the given track, d_i is the closest approach of the track to its associated hit and σ_{VD} is the estimated precision of the VD. This cut reduces the influence of wrongly associated hits in the VD.

Once a secondary vertex had been reconstructed, a second fit [12] was performed to find the most likely decay length (in two dimensions) of the B-hadron, given estimates of

- the B-hadron production point, with errors (the beamspot);
- the B-hadron decay point, with errors (the fitted vertex);
- the B-hadron flight direction (the jet momentum, which is the sum of the momenta of all tracks in the jet) as a constraint on the fit.

This decay length L was signed with respect to the jet momentum. If the reconstructed decay vertex was displaced from the beamspot in the same direction as the jet momentum then L was signed positive; otherwise L was negative. The tagging variable used in this analysis was the *signed decay length significance*, L/σ_L. The significance was used in preference to the bare decay length because it improved the efficiency at a given tagging purity. The efficiency/purity curve for folded tagging using the decay length significance is shown in figure 1(a), where the efficiency is measured after all cuts have been applied.

The impact parameter tuning used in previous DELPHI analyses [3] and described in [13] was also applied here. The excellent agreement between data and simulation for the folded L/σ_L is shown in figure 1(b). In addition to the tuning, there was also some rejection of tracks in the simulation, based on the number of associated VD hits, in order to improve the data/Monte Carlo agreement in tagging efficiency. This left a residual difference in efficiencies for three-track vertices, while if four or more tracks were required the agreement was good. While this requirement lowered the available statistics, it also reduced the systematic errors from the charm sector and thus had little effect on the total error on the measurement.

3.2 The Folded Hemisphere Double Tag Method

Each event was divided into two hemispheres by a plane perpendicular to the thrust axis. It was possible for more than one jet secondary vertex to be found in a hemisphere. In this case, the vertex with the largest absolute value of L/σ_L was used to determine whether that hemisphere was tagged.

Signing L/σ_L allowed the definition of *forward* and *backward*-tagged hemispheres. For a given placing of the cut, a hemisphere was

- forward-tagged if $L/\sigma_L >$ cut;
- backward-tagged if $L/\sigma_L < -$cut.

The folded distributions, defined as the number of forward minus backward tagged hemispheres, are shown in figure 1(b). It is evident that this folding considerably suppresses the light quark background while having little effect on the b quark distribution.

Five quantities were defined analogous to the two in normal hemisphere double tagging [1, 3]:

- F^f, the fraction of hemispheres receiving a forward tag,
- F^b, the fraction of hemispheres receiving a backward tag,
- F^{ff}, the fraction of events in which both hemispheres are forward-tagged,

- F^{bb}, the fraction of events in which both hemispheres are backward-tagged,
- F^{fb}, the fraction of events in which one hemisphere is forward-tagged and the other is backward-tagged.

Neglecting efficiency correlations between hemispheres for light and charm quarks and introducing for b quarks the correlation factor

$$\rho_b = \frac{(\epsilon_b^{ff} + \epsilon_b^{bb} - \epsilon_b^{fb})}{(\epsilon_b^f - \epsilon_b^b)^2} - 1 \tag{2}$$

leads to the equations

$$\begin{aligned} F_1 &= F^f - F^b \\ &= R_b\epsilon'_b + R_c\epsilon'_c + (1 - R_b - R_c)\epsilon'_l \qquad (3) \\ F_2 &= F^{ff} + F^{bb} - F^{fb} \\ &= R_b\epsilon'^2_b(1+\rho) + R_c\epsilon'^2_c + (1 - R_b - R_c)\epsilon'^2_l, \qquad (4) \end{aligned}$$

where $\epsilon'_q = \epsilon_q^f - \epsilon_q^b$ is the difference between the forward and backward tagging efficiencies for a quark of flavour q. The quantities ρ_b, ϵ'_c and ϵ'_l were extracted from the simulation, F_1 and F_2 from the data, and R_c was input from the Standard Model [14]. Equations (3) and (4) were then solved iteratively to measure R_b and ϵ'_b simultaneously from the data.

Due to the interplay between statistical and systematic errors, the total error on the measurement of R_b reached a minimum at a cut of $|L/\sigma_L| = 5$, as shown in figure 2. In the simulation, the b purity at this cut was about 91% and the folded tagging efficiency was about 17%. All numbers quoted below and the final result correspond to a cut at 5.

3.3 Quantities from the Simulation

Both the light and the charm quark efficiencies were extracted from the simulation, reweighted to reach the input values of various modelling parameters recommended in [14] and listed in table 1. This took account of the rate of gluon splitting to heavy quarks in light quark events, and in the charm sector of differences between the parameters used in the simulation and experimentally measured values of the charmed hadron lifetimes, production fractions and decay modes and charm fragmentation. Further reweighting was then carried out to estimate the errors on these efficiencies. There was also a small error due to limited simulation statistics. The light and charm quark folded efficiencies extracted from the simulation were:

$$\begin{aligned} (\epsilon_l^f - \epsilon_l^b) &= (0.074 \pm 0.009) \times 10^{-2}; \qquad (5) \\ (\epsilon_c^f - \epsilon_c^b) &= (1.645 \pm 0.095) \times 10^{-2}. \qquad (6) \end{aligned}$$

These are the total errors on the efficiencies and their contributions to the systematic error on R_b are broken down in table 1.

Correlations between hemispheres came from both geometrical and kinematic effects. Any non-uniformities in the efficiency of the detector could give rise to geometrical correlations. The limited polar angle acceptance of the VD and inefficient modules of this detector both had an effect. Kinematic correlations were due to the emission of hard gluons, which removed energy from both of the primary quarks and, in about 2.4% of events,

forced both B-hadrons into the same thrust hemisphere. The hemisphere correlation in b events was estimated from the simulation to be

$$\rho_b = (0.54 \pm 0.48(\text{stat}) \pm 0.61(\text{syst})) \times 10^{-2}. \quad (7)$$

The first error is due to the limited simulation statistics and the second is the estimated systematic effect.

The error on the geometrical part of the correlation was estimated by comparing the simulation and the data. Histograms of the tagging efficiency as a function of $\cos\theta$ or ϕ of the jet momentum were constructed and the total single (ϵ) and double (ϵ^d) tagging efficiencies were calculated from them. The correlation due to each angular source was then obtained from these total efficiencies using the relation $\rho = \frac{\epsilon^d}{\epsilon^2}$. The larger of the difference between the data and simulation correlations or the statistical error on this difference was taken as an estimate of the systematic error due to each angular source.

For the error due to QCD effects, the prescription in [14] was followed. The mean B-hadron lifetime was varied within the range (1.55 ± 0.05) ps and found to have little effect on the correlation. This analysis made use of the beamspot instead of reconstructing a primary vertex for each event. Use of an averaged beamspot position was also found, as expected, to have a negligible effect on the calculated correlation. This is not the case for analyses using a fitted primary vertex, which leads to an additional source of systematic uncertainty.

3.4 Results of the Secondary Vertex Analysis

Using the numbers of hemispheres and events tagged in the data and the values for the efficiencies and correlations given above, and taking into account the small selection bias towards $Z \rightarrow b\overline{b}$ events mentioned in section 2, R_b was calculated to be:

$$R_b = 0.2176 \pm 0.0028(\text{stat}) \pm 0.0027(\text{syst}) - 0.029\frac{R_c - 0.172}{0.172}. \quad (8)$$

The folded b-tagging efficiency calculated simultaneously from the data was $(17.29 \pm 0.22)\%$, compared to 17.16% in the simulation.

A value of R_b was also obtained without applying the tuning referred to in section 3.1, but still with the track rejection in place, and the two results compared. Half of the difference was assigned as a conservative estimate of the error due to detector resolution effects. Similarly, R_b was determined when a further 2% of the tracks were randomly rejected and half of the difference between this and the central value was taken as an estimate of the error due to any residual disagreement between the data and Monte Carlo multiplicity distributions. These contributions are combined in quadrature for the quoted detector resolution error. A full breakdown of the systematic error on R_b is shown in table 1.

The stability of the measurement over a range of cuts on L/σ_L is demonstrated in figure 3.

4 Combination of the Results

The result of this analysis has been combined with the previous DELPHI result [3], taking into account the common systematic errors. The breakdown of the errors for the individual

analyses and for the combination is given in table 1. The errors within a line have been assumed to be fully correlated, except for the detector effects which are correlated within each year's data set and uncorrelated between years. The statistical correlation between the mixed tag and the other analyses can be neglected. The correlation between the double impact parameter tag and the multivariate analysis has been estimated using a Monte Carlo technique to be less than 0.35 (90% C.L.). Conservatively this value has been used in the average[2]. The combined result is:

$$R_b = 0.2202 \pm 0.0014(\text{stat}) \pm 0.0018(\text{syst}) - 0.010\frac{R_c - 0.172}{0.172},$$

with $\chi^2/ndf = 1.2/2$.

		Uncertainty $\times 10^4$				
Error Source	Range	dit	mt	mult	vert	com
Internal experimental effects:						
Hemisphere correlations		$\pm$ 10	0	$\pm$ 12.2	$\pm$ 16	$\pm$ 7
Lepton-vertex correlations		0	$\pm$ 12	0	0	$\pm$ 3
Detector effects		$\pm$ 9	$\pm$ 9	$\pm$ 6.8	$\pm$ 6	$\pm$ 6
Lepton sample purity		0	$\pm$ 19	0	0	$\pm$ 3
Acceptance bias		$\pm$ 2	$\pm$ 2	$\pm$ 2.7	$\pm$ 2	$\pm$ 1
Method		0	0	$\pm$ 14.5	0	$\pm$ 4
$\langle x_E(b)\rangle$	0.702 ± 0.008	$\mp$ 9.0	0	$\mp$ 1.5	0	$\mp$ 3.1
$\langle x_E(c)\rangle$	0.484 ± 0.008	$\mp$ 3.0	$\mp$ 3.0	$\mp$ 0.6	$\mp$ 3.1	$\mp$ 2.3
Br($c \to \ell$)	$(9.8 \pm 0.5)\%$	0	$\pm$ 10.0	0	0	$\pm$ 1.6
Semilept. model $b \to \ell$ [7]	$(^{+\text{ACCMM}}_{-\text{ISGW}**})$	0	$\pm$ 11.0	0	0	$\pm$ 1.8
Semilept. model $c \to \ell$ [7]	ACCMM1 $(^{+\text{ACCMM2}}_{-\text{ACCMM3}})$	0	$\mp$ 8.0	0	0	$\mp$ 1.3
D^0 lifetime	0.415 ± 0.004 ps	$\mp$ 1.5	$\mp$ 1.0	$\mp$ 0.3	$\mp$ 1.4	$\mp$ 1.0
D^+ lifetime	1.057 ± 0.015 ps	$\mp$ 2.6	$\mp$ 1.3	$\mp$ 0.2	$\mp$ 0.2	$\mp$ 1.2
D_s lifetime	0.467 ± 0.017 ps	$\mp$ 1.8	$\mp$ 1.2	$\mp$ 0.4	$\mp$ 0.7	$\mp$ 1.0
Λ_c lifetime	0.206 ± 0.012 ps	$\mp$ 0.0	$\mp$ 0.0	$\mp$ 0.7	$\mp$ 0.3	$\mp$ 0.3
B lifetime	1.55 ± 0.05 ps	$\mp$ 3.0	$\mp$ 0.0	$\mp$ 3.4	$\mp$ 1.0	$\mp$ 2.1
B decay multiplicity	5.73 ± 0.35	$\pm$ 9.0	$\pm$ 0.0	$\pm$ 1.8	$\pm$ 0.0	$\pm$ 3.2
D decay multiplicity	2.39 ± 0.14	$\mp$ 6.0	$\mp$ 4.0	$\mp$ 0.2	$\mp$ 8.5	$\mp$ 4.6
$BR(D \to K^0 X)$	0.46 ± 0.06	$\pm$ 8.0	$\pm$ 7.0	$\pm$ 5.0	$\pm$ 12.9	$\pm$ 6.9
$g \to c\overline{c}$	$(2.38 \pm 0.48)\%$	$\mp$ 3.0	$\mp$ 3.0	$\pm$ 0.2	$\mp$ 4.8	$\mp$ 2.5
$g \to b\overline{b}$	$(0.13 \pm 0.04) \times (g \to c\overline{c})$	$\mp$ 3.0	$\mp$ 3.0	$\mp$ 0.1	$\mp$ 3.2	$\mp$ 2.2
Light hadron modelling	tuned JETSET $\pm$ 10%	$\mp$ 6.0	$\mp$ 5.0	$\mp$ 0.4	$\mp$ 2.0	$\mp$ 3.3
QCD hemisphere correlations	see text	$\pm$ 9.0	$\pm$ 5.0	$\pm$ 4.4	$\pm$ 5.9	$\pm$ 6.3
D^+ fraction	0.231 ± 0.026	$\mp$ 10.6	$\mp$ 5.2	$\mp$ 0.4	$\mp$ 1.7	$\mp$ 5.0
D_s fraction	0.110 ± 0.017	$\mp$ 1.1	$\mp$ 2.0	$\mp$ 1.2	$\mp$ 0.0	$\mp$ 2.3
c-baryon fraction	0.063 ± 0.029	$\pm$ 2.6	$\pm$ 2.6	$\pm$ 0.8	$\pm$ 6.5	$\pm$ 2.5

Table 1: Summary of systematic errors on R_b obtained from the double impact parameter tag (dit), the mixed tag (mt) and the multivariate tag (mult) for 1991–93 data and for the secondary vertex tag (vert) for 1994, and the combination of the analyses (com). Detailed explanations of how the different error sources are obtained can be found in [7].

[2]The most probable value for the correlation was found to be 0. It has been checked that the final result does not change using this value.

Because of the different charges of up-type and down-type quarks, a correction of $+0.0003$ due to photon exchange has to be applied to obtain R_b^0 from R_b [15], resulting in

$$R_b^0 = 0.2205 \pm 0.0014(\text{stat}) \pm 0.0018(\text{syst}) - 0.010\frac{R_c - 0.172}{0.172}.$$

5 Conclusions

A different measurement of the partial decay width R_b^0 of the Z into $b\overline{b}$ quark pairs has been performed. Events were selected according to the displacement of reconstructed secondary vertices from the beamspot. The following result was obtained:

$$R_b = 0.2176 \pm 0.0028(\text{stat}) \pm 0.0027(\text{syst}) - 0.029\frac{R_c - 0.172}{0.172}.$$

Combining this number with the previous published one, the result is:

$$R_b^0 = 0.2205 \pm 0.0014(\text{stat}) \pm 0.0018(\text{syst}) - 0.010\frac{R_c - 0.172}{0.172}.$$

For this number, all centre of mass energies at which LEP has run have been combined. All results are in agreement with those of other measurements at LEP and at SLD [1, 2, 4, 5, 6]. Assuming a mass of the top quark of $m_t = 175 \pm 12$ GeV/c^2, as obtained from a simple average of the CDF [16] and the D0 [17] measurements, the Standard Model predicts $R_b^0 = 0.2155 \mp 0.0005$ [15]. This number is about 2.2 standard deviations lower than our measurement, assuming $R_c = 0.172$.

Acknowledgements

We are greatly indebted to our technical collaborators and to the funding agencies for their support in building and operating the DELPHI detector, and to the members of the CERN-SL Division for the excellent performance of the LEP collider.

References

[1] ALEPH Collaboration, D. Buskulic et al., Phys. Lett. **B313** (1993) 535.

[2] ALEPH Collaboration., D. Buskulic et al., Phys. Lett. **B313** (1993) 549.

[3] DELPHI Collaboration, P. Abreu et al., Z. Phys. **C70** (1996) 531.

[4] L3 Collaboration, O. Adriani et al., Phys. Lett. **B307** (1993) 237.

[5] OPAL Collaboration, P.D. Acton et al., Z. Phys. **C65** (1995) 17,
OPAL Collaboration, P.D. Acton et al., Physics note PN181, EPS-0278 (1995).

[6] SLD Collaboration,SLAC-PUB-7170, May 1996. Presented by Erez Etzion at 31st Rencontres de Moriond: Electroweak Interactions and Unified Theories, Les Arcs, France, 16-23 Mar 1996. e-Print Archive: hep-ex/9606008

[7] The LEP collaborations, *Combination of Heavy Flavour Electroweak Measurements at LEP*, LEPEWWG 96-01.

[8] DELPHI Collaboration, P. Aarnio et al., Nucl. Inst. Meth. **A303** (1991) 233.

[9] DELPHI Collaboration, P. Abreu et al., *Performance of the DELPHI detector*, CERN-PPE/95-194, submitted to Nucl. Inst. Meth.

[10] T. Sjöstrand et al., in *"Z physics at LEP 1"*, CERN 89-08, CERN, Geneva, 1989; Comp. Phys. Comm. **39** (1986) 347.

[11] DELSIM reference manual, DELPHI 87-98 PROG 100, Geneva, 1989.

[12] G.J.Barker, *A Measurement of the Mean B-Hadron Lifetime Using the Central Drift Chambers of the OPAL Experiment at LEP*, Ph.D. Thesis, Queen Mary and Westfield College, University of London.

[13] G.Borisov and C.Mariotti, Nucl. Inst. Meth. **A372** (1996) 181.

[14] The LEP Electroweak Working Group, *Presentation of LEP Electroweak Heavy Flavour Results for Summer 1996 Conferences*, LEPHF/96-01, ALEPH Note 96-99, DELPHI 96-67 PHYS 627, L3 Note 1969, OPAL Technical Note TN391.

[15] D. Bardine et al., *ZFITTER: An Analytical Program for Fermion Pair Production in e^+e^- Annihilation*, CERN-TH 6443/92 (May 1992).

[16] CDF Collaboration, F. Abe et al., Phys. Rev. Lett. **74** (1995) 2626.

[17] DØ Collaboration, S. Abachi et al., Phys. Rev. Lett. **74** (1995) 2632.

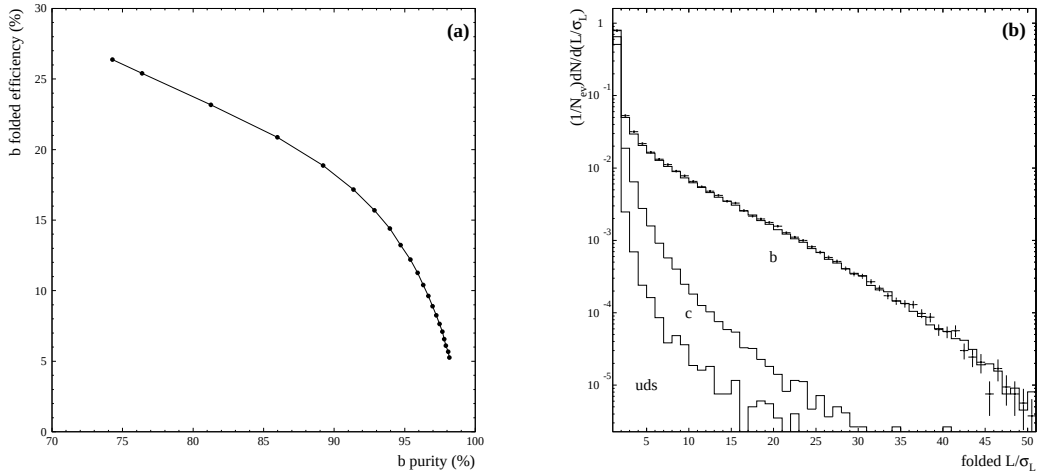

Figure 1: (a) Efficiency/purity curve for tagging b hemispheres in the simulation. (b) Folded L/σ_L distributions in simulation and data. Distributions are normalised by the total number of forward minus backward hemispheres in the simulation/data, as appropriate.

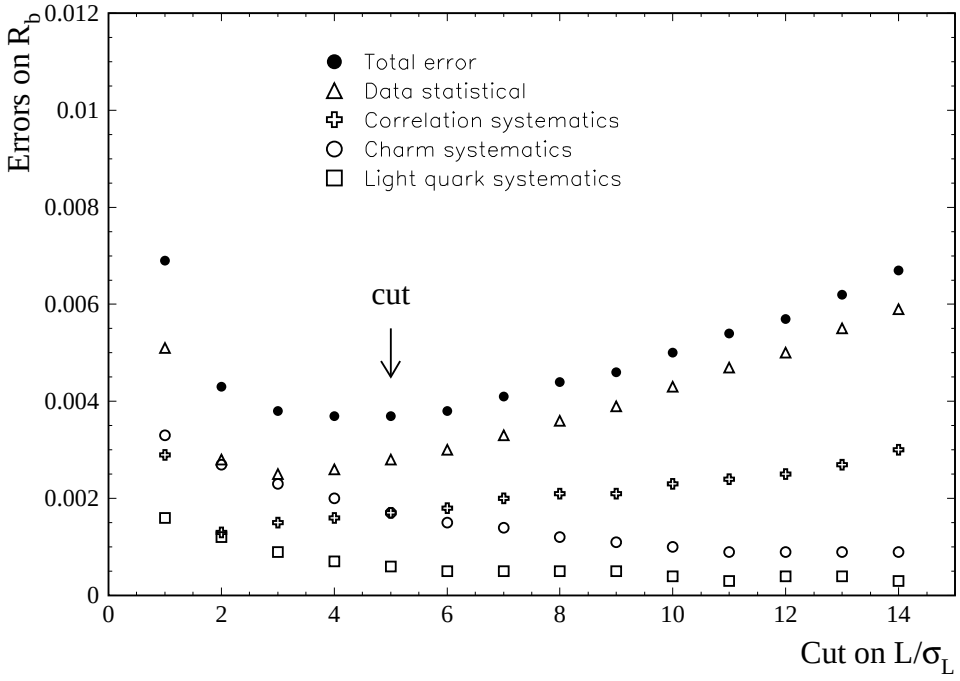

Figure 2: Contributions to the error on R_b. The arrow marks the position of the cut.

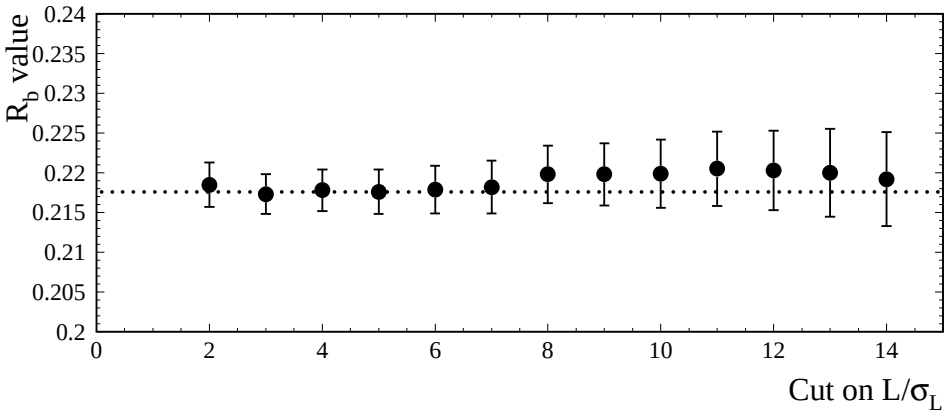

Figure 3: The measured value of R_b as a function of the cut on the L/σ_L for 1994. The errors are statistical only and are correlated from point to point. The line shows the value at a cut of 5.